To deliver the magnetic carriers to the specific target tumors other than liver, surface functionalization by polyethyeleneglycol (PEG) (the so-called PEGylation) is necessary to give the stealthy character to the nanoparticles. Polyethyeleneglycol is used with a number of nanoparticles as it improves colloidal stability and prevents uptake by the reticuloendothelial system (Wang and Thanou 2006). PEG is usually added onto the surface of nanoparticles to create the steric stabilization effect where the PEG molecules form a protective hydrophilic layer on the surface of nanoparticles that prevents aggregation and nonspecific adsorption of blood components. As a conventional method, Kohler successfully synthesized PEGylated SPIO using PEG silane which is covalently bound to iron-oxide surface (Kohler et al. 2004). However, the toluene used as a reaction solvent is not preferable from the viewpoint of biocompatibility. Other conventional methods such as co-precipitation method or crosslinking method are considered to be unstable when compared with chemical bonding process. Facile, stable, and biocompatible PEGylation process is expected. Another point to be considered for in vivo applications is the hydrodynamic particle size in the blood stream. To avoid the body's reticuloendothelial system (RES), mainly the kupffer cells in the liver and expect the effective expression of EPR effect, hydrodynamic size of the iron-oxide nanoparticles should be controlled within the range of 10–100 nm (Davis et al. 2008).

We have already reported that Au/Feridex composite nanoparticle synthesized by radiochemical process modified with PEG via Au–S bonding showed lower uptake by the liver and higher accumulation in the tumor than Feridex alone (Kojima et al. 2010). However, the hydrodynamic size of the PEG/Au/Feridex was ca. 150 nm, which should be decreased for the construction of effective delivery system. In this article, we report on the design of composite nanoparticle consisting of Au and SPIO for more effective delivery system. The hydrodynamic sizes were controlled by changing the stabilizing polymer and SPIOs used as starting materials. The Au nanoparticles on SPIOs have surface functionality of Au–S bonding, which enables easy and facile surface modification (Kinoshita et al. 2005; Kojima et al. 2010). The surface of the composite nanoparticle was PEGylated by simply mixing with thiol-modified polyethylene glycol via Au–S bonding.

Experimental procedure

Chemicals

Two kinds of SPIOs, Resovist® and Moday ION™ (BioPhysics Assay Laboratory, Inc.) commercialized as MR contrast agents are used for magnetic carriers. Resovist® mainly composed of γ-Fe_2O_3 nanoparticles coated with carboxydextran and developed as a liver-specific MR contrast agent. Molday-ION is mainly composed of Fe_3O_4 nanoparticles and developed as Blood pool agent. Both the Resovist® and Molday-ION™ have strong effects on the shortening of T_2 relaxation times. Hydrodynamic particle size ranges of raw Resovist and Molday-ION in water systems are 45–60 and 30 nm, respectively. These SPIOs are too small to apply conventional magnetic separation technique even with NEOMAX®, the strongest permanent magnet.

Millipore Direct-Q system was used to obtain pure water in all systems. Chemicals such as $HAuCl_4$ and 2-propanol were purchased from Wako Pure Chemical Industries Ltd. Polymers of polyvinyl alchol (PVA, MW = 22 kDa), polyvinyl pyrrolidone (PVP, MW = 40 kDa), and (PMMA, MW = 100 kDa) were purchased from Wako Pure Chemical Industries Ltd. and used for controlling the Au particle size. In addition, thiol-modified polyethylene glycol (PEG-SH, MW = 5 kDa) was purchased from NOF Corp. and used for the PEGylation of Au/SPIO composite surface.

Synthesis of Au/SPIO composite nanoparticles

The Au/SPIO composite nanoparticles were synthesized by radiochemical procedure (Seino et al. 2008). In this process, the composite nanoparticles were synthesized in aqueous solution system without harmful surfactants, organic solvents, heat treatments, and drying process. Consequently, the composite nanoparticle is expected to show good dispersibility and biocompatibility. The SPIO of 5 mg were dispersed in 50 mL of aqueous solution containing $HAuCl_4$, 2-propanol and polymer. Concentrations of $HAuCl_4$ and 2-propanol were 0.5 and 125 mM. Polymer concentration was controlled to 10 g/L for PVA and 1 g/L for others. The dispersion was irradiated with high-energy electron beam (4.8 MeV, Japan Electron Beam Irradiation Service, Ltd.) at dose rate of 3 kGy/s for 2 s.

Purification of Au/SPIO composite nanoparticles

After the irradiation, Au/SPIOs were purified by high-speed ultracentrifugation process or dialysis process. The ultracentrifugation was used to spin down composite nanoparticles with relative centrifugal force of $1.0–1.4 \times 10^5 \times g$ for 2 h. The samples were re-suspended in pure water using bath sonicator. With dialysis process, the sample dispersion was sealed in dialysis membrane (Spectra/Por®, MWCO = 100 kDa, Spectrum Laboratories, Inc.) and kept in pure water for 48 h at room temperature.

PEGylation of the Au/SPIO composite nanoparticles

Aqueous suspension of the Au/SPIO composite nanoparticles was mixed with PEG-SH solution. In this experiment, excess amounts of PEG-SH were applied to modify all the Au surfaces via Au–S bonding (20 μmol PEG-SH/mg-Au). The mixture was incubated at room temperature for 1 h and then purified by centrifugation ($1.0 \times 105 \times g$, 30 min.). Amounts of the PEG-SH combined with Au/SPIO composites were determined by ICP-AES and thermogravimetric analysis (TGA50, Shimadzu Corp.).

Material characterization

Morphology of the samples was investigated using a transmission electron microscope (TEM; HITACHI, H-8100, 200 kV). Hydrodynamic particle sizes of the Au/SPIO composites were characterized using Zetasizer Nano (Malvern Instruments Ltd). Atomic ratio of gold to iron analyzed by ICP-AES using ICPS7500 (Shimadzu Corp.). To confirm the Au–S bonding ability of the Au/SPIO composites, amounts of amino acids adsorbed onto the nanoparticles were measured with amino acid analyzer, L-8500A (Hitachi High-Tech. Corp.). The composite nanoparticles were mixed with 17 kinds of alpha-amino acids in 0.02 N HCl aqueous solutions. The solution was mixed for 2 h at room temperature, and then separated by a centrifugation. The detailed procedure for the measurement is reported elsewhere (Kinoshita et al. 2005).

Durability of the Au/SPIO composites in blood serum system was evaluated also by estimating the amount of nanoparticles dispersed in the solution by UV–Vis absorption spectroscopy. UV–Vis absorption spectra were measured by a spectrometer, Cary 50 (Varian Inc.). The detailed process is already reported elsewhere (Seino et al. 2009). UV–Vis absorption spectra of the Au/SPIO showed surface plasmon resonance due to nanosized Au nanoparticles around a wavelength of 540 nm, which decreased with the sedimentation of Au/SPIO. The concentration of Au/SPIO in blood serum at the elapsed time t is estimated by the absorption reduction rate as follows:

$$\text{Au/SPIO concentration}\,(t) = \text{Abs}_{540\,\text{nm}}\,(t)/\text{Abs}_{540\,\text{nm}}\,(0).$$

Results and discussion

Morphology and dispersibility of the Au/SPIO composite nanoparticles

After the electron beam irradiation, the color of the suspensions changed from brown/black (color of SPIOs) to reddish color, indicating the formation of Au nanoparticles. Surface plasmon resonances due to nanosized Au particles were observed by UV–Vis absorption spectroscopy (data not shown.). Figure 1 shows the typical TEM images of the typical Au/SPIO composite nanoparticles. It was observed that Au nanoparticles (seen as darker contrast) are supported on the iron-oxide nanoparticles (seen as weaker contrast) to form Au/SPIO composite nanoparticles. Primary particle sizes of Resovist and Molday-ION are about 10 nm. Geometric average sizes and geometric standard deviations of Au nanoparticles determined by measuring the Au size from several TEM micrographs are summarized in Table 1. Sizes of Au grains were well controlled by the coexisting polymers. It was indicated that polymers of PVP and PMMA are also applicable to radiochemical synthesis as surface stabilizer. Average diameters of the Resovist and Molday-ION were about 5 nm. It was noticed that the Au/SPIO composites do not exist as monodispersed nanoparticles, but as small aggregates. The sizes of the aggreagtes of Au/Moday ION seem smaller than that of Au/Resovist.

Hydrodynamic particle sizes of the Au/SPIO composites before and after the centrifugal purification are tabulated in Table 1. Hydrodynamic particle sizes of Au/Resovist decreased from 200–280 to 140–170 nm by purification process. Removal of excess polymer was effective for the decrement of hydrodynamic

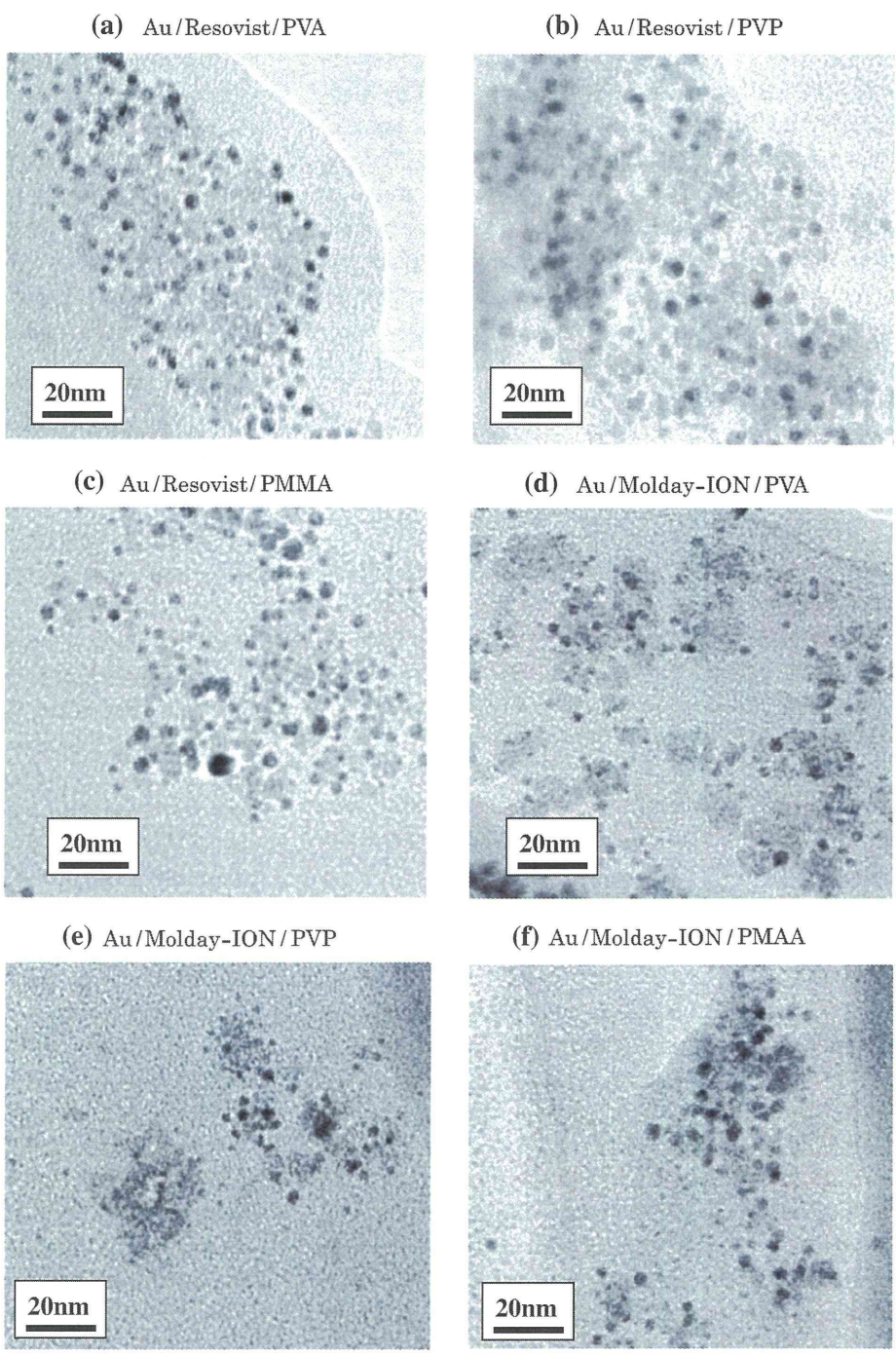

Fig. 1 TEM images of the Au/SPIO composite nanoparticles.
a Au/Resovist/PVA,
b Au/Resovist/PVP,
c Au/Resovist/PMMA,
d Au/Molday-ION/PVA,
e Au/Molday-ION/PVP,
f Au/Molday-ION/PMMA

particle size. Hydrodynamic sizes of Au/Molday-IONs were relatively smaller than Au/Resovists. It is assumed that smaller hydrodynamic particle size of raw Molday-ION (30 nm) than raw Resovist (45–60 nm) resulted in smaller Au/SPIO size.

Hydrodynamic sizes of Au/Molday-ION composites synthesized with PVA increased from 50 to 71 nm by centrifugal process, which implies the formation of larger aggregates by centrifugal force. Figure 2 shows the hydrodynamic particle size histograms of Au/Molday-ION composite nanoparticles before and after the purification by centrifugal process or dialysis process. The light-scattering intensity-weighted frequency is plotted against the hydrodynamic particle

Table 1 Au particle sizes and hydrodynamic sizes of Au/SPIO composite nanoparticles

Mag. carrier	Polymer	Au nanoparticle		Hydrodynamic size in water	
		Ave. size (nm)	SD	Before purification (nm)	After purification (nm)
Resovost	PVA (10 g/L)	3.6	1.3	282	137
	PVP (1 g/L)	4.1	1.2	199	171
	PMMA (1 g/L)	3.3	1.4	236	177
Molday-ION	PVA (10 g/L)	3.4	1.3	50	71
	PVP (1 g/L)	2.9	1.3	122	No data
	PMMA (1 g/L)	3.3	1.3	88	No data

sizes. The histograms slightly shift to larger sizes by both purification processes. It should be noticed here that agglomerates larger than 1 μm were formed by the centrifugal process, while dialysis membrane separation process not. It was indicated that dialysis membrane separation process is effective to avoid aggregation during purification system.

Surface activity of Au/SPIO composite nanoparticles

Surface activity of Au grains in Au/SPIO composites were examined by adsorption of sulfur-containing amino acids. Figure 3 shows the adsorbed amounts of each amino acid to the Au/Resovist composite nanoparticles synthesized with PVA, PVP, or PMMA. The adsorbed amounts are normalized to 1 mg of γ-Fe_2O_3 contained in composites. It should be noticed that remarkably high amounts of cystine and methionine including sulfur were absorbed among them all in all composites. Table 2 shows the sum total of adsorbed sulfur-containing amino acids and non-sulfur amino acids onto composite nanoparticles. The values obtained with cystine are doubled, as it is a dimer of the cysteine and have two sulfur atoms to bind Au surface. It was clearly shown that the Au nanoparticles in composites have strong affinity to the sulfur-containing amino acids. These results are almost consistent with the previous reports, in which composite nanoparticles are synthesized by using magnetic particle sizes of 20–100 nm (Kinoshita et al. 2005). The last column shows the specificity of each composites, assuming that adsorption of sulfur-containing amino acids are specific via Au–S bonding and adsorption of non-sulfur amino acids are nonspecific. The composite obtained with PVA showed highest value among tested samples. The difference in specificity is assumed to be caused by several factors, such as morphology of the composites (size, Au/Fe ratio, dispersibility, etc.) and conditions of remaining polymers on composites (amount, surface coverage, effect of ionizing radiation, etc.).

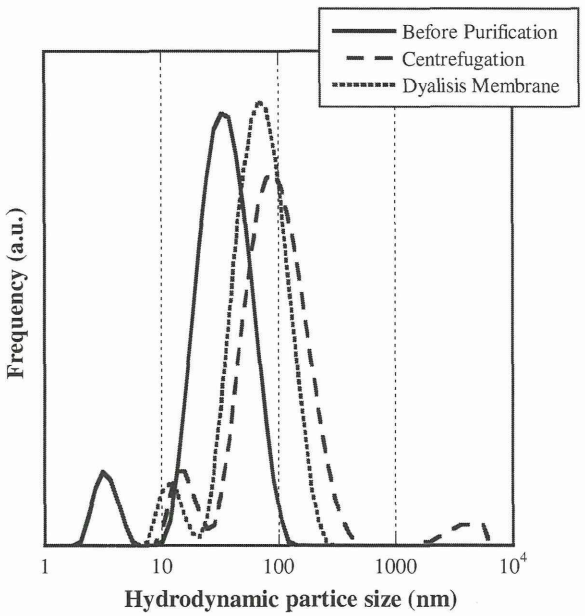

Fig. 2 Hydrodynamic particle size distributions of Au/Molday-ION composite nanoparticles

PEGylation of the Au/SPIO composites were demonstrated by using Au/Molday-ION composite nanoparticles synthesized by using PVA. Hydrodynamic particle size of PEGylated Au/Molday-ION in water system was 67 nm, slightly 56 nm. It was assumed that the PEG chains adsorbed onto composites via Au–S bonding slightly enlarged the hydro dynamic particle sizes. Figure 4 shows the thermogravimetric analysis data of Au/SPIO composite nanoparticles before and after the PEGylation by

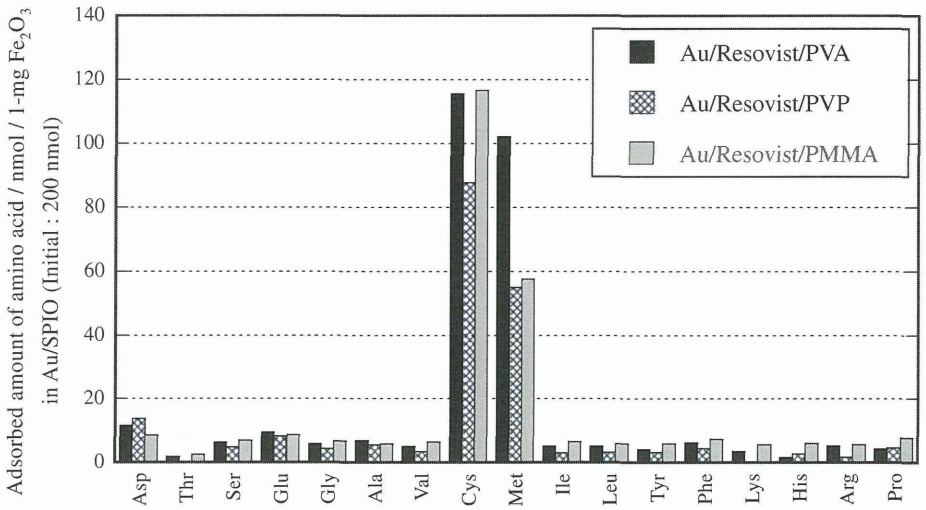

Fig. 3 Amount of adsorbed amino acids onto Au/Resovist composite nanoparticles

Table 2 Sum total of adsorbed amino acids onto Au/Resovist composite nanoparticles

Sample ID	Sum total of adsorbed amino acids (nmol/Fe_2O_3 1 mg)		Specificity
	Sulfur containing	No sulfur	
Au/Resovist/PVA	333	82	4.1
Au/Resovist/PVP	230	63	3.7
Au/Resovist/PMMA	291	96	3.0

PEG-SH. Before the PEGylation, the weight is decremented to 87.5 %, which indicated the existence of surface residual PVA. After the surface modification by PEG-SH, the weight is decremented to 76.1 %, which indicated that the PEG was strongly adsorbed onto Au nanoparticles via Au–S bonding. The amount of PEG-SH adsorbed onto Au/Molday-ION was 89 nmol/mg, which was almost consistent with the result that determined by ICP measurement (measurement of sulfur content together with Fe and Au). From these results, number of the PEG-SH chains modified on one Au particle is estimated as ca. 15.

Surface activities of the Au NPs on SPIOs against sulfur-containing amino acids and PEG-SH are discussed by comparing the surface coverage of these molecules on the surface area of the gold grains. Surface coverage of sulfur-containing amino acids onto Au/Resovist/PVA was 398 pmol/cm^2-Au and of PEG-SH was 66 pmol/cm^2-Au (Au/Molday-ION/PVA). These values are relatively higher than the values obtained with

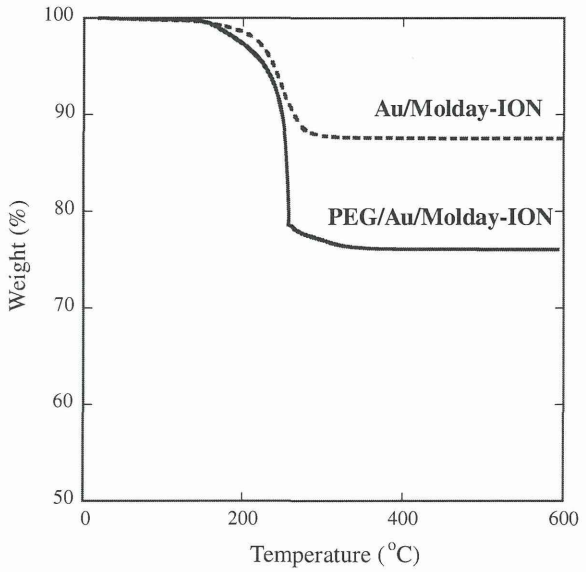

Fig. 4 Thermogravimetric analysis data of Au/SPIO composite nanoparticles before and after the PEGylation

hybridized 15-mer oligonucleotides and Au/Iron-oxide composites, 2.0–2.5 pmol/cm^2 (Kinoshita et al. 2007). It is reasonable to consider that smaller molecules of amino acids (121.16 Da with cysteine and 149.21 Da with methionine) have higher Au–S activity than larger molecules such as PEG-SH (5 kDa) and hybridized oligonucleotides modified with FITC (10.6 kDa). Lower affinity against oligonucleotide might be attributed to the effect of steric hindrance of hybridized oligonucleotide and/or of electrostatic repulsion. To summarize, it was indicated that the surfaces of Au nanoparticles have high

Au–S binding affinity and can be used for the surface modification of Au/SPIO composites.

Stability of the Au/SPIO composite nanoparticles in blood serum

Stabilities of the Au/SPIO composite nanoparticles in blood systems were estimated by the following in vitro experiments. The Au/SPIO composites purified by centrifugal process (Au/Resovist) or dialysis process (Au/Molday-ION) were re-dispersed in beef blood serum. Table 3 shows the hydrodynamic particle sizes of Au/SPIO composites in blood serum and in water. It was indicated that the Au/SPIO composites showed good dispersibility even in blood serum. Hydrodynamic sizes of Au/Molday-ION composites were significantly smaller than that obtained with Au/Resovist composites, which attributed to the smaller hydrodynamic size of raw Molday-ION. It should be noticed here that hydrodynamic particle size of PEGylated Au/Molday composite was 65 nm even in blood serum.

In Fig. 5, Au/SPIO concentrations in blood serum system are plotted against the elapsed time. It was indicated that more than 90 % of Au/SPIO composites were still dispersed even in the blood serum at the elapsed time of 50 min. It was also confirmed that hydrodynamic particle sizes of Au/SPIOs were almost same before and after the durability test. The Au/Molday-ION composites showed higher stability compared with Au/Resovist composites, which probably due to the smaller hydrodynamic particle size. Especially, PEGylated Au/Molday-ION composites showed the best result, that more than 99 % of the nanoparticles kept suspended. As the blood circulating time is just a few minutes, the PEGylated Au/Molday-ION is expected to be delivered to whole body without causing a thrombus in blood capillaries. We have also confirmed that Au nanoparticles and polymers on SPIOs do not affect the T2 relaxation efficiency (Kojima et al. 2010 and unpublished results). These results indicate that the present composite nanoparticles can be good candidates for the in vivo applications.

Table3 Hydrodynamic sizes of Au/SPIO composite nanoparticles in water or blood serum

Sample ID	Hydrodynamic size (nm)	
	In water	In blood serum
Au/Resovist (PVA)	137	90
Au/Resovist (PVP	171	142
Au/Resovist/PMMA	177	205
Au/Molday-ION/PVA	56	55
PEGylated/Au/Molday-ION	67	65

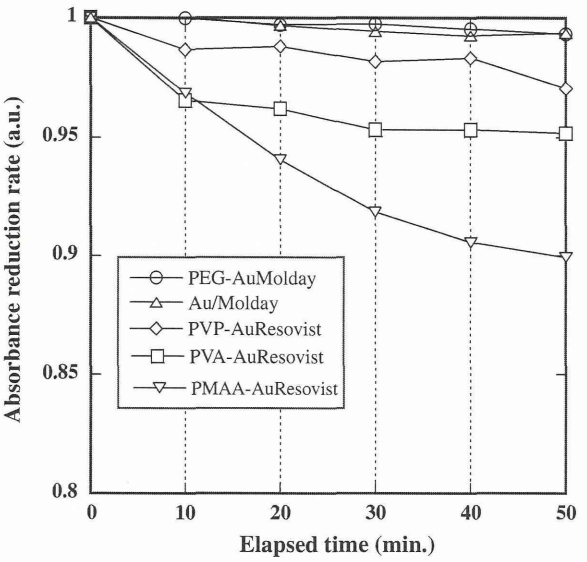

Fig. 5 Stability of the Au/SPIO composites in blood serum

Conclusion

The Au/SPIO composite nanoparticles were successfully synthesized by radiochemical process by keeping the dispersibility of raw SPIOs. As a stabilizing polymer, the use of PVA seems to be the most highly suited for smaller hydrodynamic particle size of Au/SPIO composite nanoparticles. The Au nanoparticle on SPIO kept the specific binding affinity via Au–S bonding, which enabled facile and stable surface functionalization by PEG-SH. The PEGylated Au/SPIO showed excellent dispersibility in blood serum with hydrodynamic particle size was 65 nm. The PEGylated Au/SPIO is expected to avoid RES uptake and express EPR effect, which are promising features for applications in future in vivo studies.

Acknowledgments This study was partially supported by the Japan Science and TechnologyAgency (JST). The authors thank K. Ueno (EBIS, Japan) for sparing his precious time during the operation of the electron accelerator.

References

Allen TM, Cullis PR (2004) Science 303:1818–1822

Balmayor ER, Azevedo HS, Reis RL (2011) Pharm Res 28:1241–1258

Davis ME, Chen Z, Shin DM (2008) Nat Rev Drug Discov 7:771–782

Gupta AK, Gupta M (2005) Biomaterials 26:3995–4021

Kinoshita T, Seino S, Mizukoshi Y, Otome Y, Nakagawa T, Okitsu K, Yamamoto TA (2005) J Magn Magn Mater 293:106–110

Kinoshita T, Seino S, Mizukoshi Y, Nakagawa T, Yamamoto TA (2007) J Magn Magn Mater 311:255–258

Kohler N, Fryxell GE, Zhang M (2004) J Am Chem Soc 126:7206–7211

Kojima H, Mukai Y, Yoshikawa M, Kamei K, Yoshikawa T, Morita M, Inubushi T, Yamamoto TA, Yoshioka Y, Okada N, Seino S, Nakagawa S (2010) Bioconj Chem 21:1026–1031

Mitchell DG (1999) MRI principles. W.B. Saunders Company, Philadelphia

Mornet S, Vasseur S, Grasset F, Duguet E (2004) J Mater Chem 14:2161–2175

Neuberger T, Schopf B, Hofmann H, Hofmann M, Rechenberg B (2005) J Magn Magn Mater 293:483–486

Seino S, Kinoshita T, Nakagawa T, Kojima T, Taniguchi R, Okuda S, Yamamoto TA (2008) J Nanopart Res 10:1071–1076

Seino S, Matsuoka Y, Kinoshita T, Nakagawa T, Yamamoto TA (2009) J Magn Magn Mater 321:1404–1407

Wang M, Thanou M (2006) Pharmacol Res 62:90–99

Weinstein JS, Varallyay CG, Dosa E, Gahramano S, Hamilton B, Rooney WD, Muldoon LL, Neuwelt EA (2010) J Cereb Blood Flow Metab 30:15–35

Cytokine 61 (2013) 578–584

Contents lists available at SciVerse ScienceDirect

Cytokine

journal homepage: www.journals.elsevier.com/cytokine

Mutants of lymphotoxin-α with augmented cytotoxic activity *via* TNFR1 for use in cancer therapy

Tomohiro Morishige [a,1], Yasuo Yoshioka [b,c,*,1], Shogo Narimatsu [a], Shinji Ikemizu [d], Shin-ichi Tsunoda [c,e], Yasuo Tsutsumi [b,c,e], Yohei Mukai [a], Naoki Okada [a], Shinsaku Nakagawa [a,c,*]

[a] *Laboratory of Biotechnology and Therapeutics, Graduate School of Pharmaceutical Sciences, Osaka University, 1-6 Yamadaoka, Suita, Osaka 565-0871, Japan*
[b] *Laboratory of Toxicology and Safety Science, Graduate School of Pharmaceutical Sciences, Osaka University, 1-6 Yamadaoka, Suita, Osaka 565-0871, Japan*
[c] *The Center for Advanced Medical Engineering and Informatics, Osaka University, 1-6 Yamadaoka, Suita, Osaka 565-0871, Japan*
[d] *Graduate School of Pharmaceutical Sciences, Kumamoto University, 5-1 Oe-honmachi, Kumamoto 862-0973, Japan*
[e] *Laboratory of Biopharmaceutical Research, National Institute of Biomedical Innovation, 7-6-8 Saito-Asagi, Ibaraki, Osaka 567-0085, Japan*

ARTICLE INFO

Article history:
Received 6 July 2012
Received in revised form 29 September 2012
Accepted 6 November 2012
Available online 11 December 2012

Keywords:
Affinity
Apoptosis
Bioactivity
Cytokine
Cytotoxicity

ABSTRACT

The cytokine lymphotoxin-α (LTα) is a promising candidate for use in cancer therapy. However, the instability of LTα *in vivo* and the insufficient levels of tumor necrosis factor receptor 1 (TNFR1)-mediated bioactivity of LTα limit its therapeutic potential. Here, we created LTα mutants with increased TNFR1-mediated bioactivity by using a phage display technique. We constructed a phage library displaying lysine-deficient structural variants of LTα with randomized amino acid residues. After affinity panning, we screened three clones of lysine-deficient LTα mutant, and identified a LTα mutant with TNFR1-mediated bioactivity that was 32 times that of the wild-type LTα (wtLTα). When compared with wtLTα, the selected clone showed augmented affinity to TNFR1 due to slow dissociation rather than rapid association. In contrast, the mutant showed only 4 times the TNFR2-mediated activity of wtLTα. In addition, the LTα mutant strongly and rapidly activated caspases that induce TNFR1-mediated cell death, whereas the mutant and wtLTα activated nuclear factor-kappa B to a similar extent. Our data suggest that the kinetics of LTα binding to TNFR1 play an important role in signal transduction patterns, and a TNFR1-selective LTα mutant with augmented bioactivity would be a superior candidate for cancer therapy.

1. Introduction

Lymphotoxin-alpha (LTα) is a tumor necrosis factor (TNF) superfamily cytokine with tumor-cell-specific cytotoxic activity and immune-activating activity. LTα induces the expression of chemokines and adhesion molecules in endothelial cells, and plays a key role in lymph node neogenesis [1–3]. Schrama et al. [4,5] showed that systemic administration of LTα to a tumor-bearing mouse leads to the construction of ectopic lymphoid tissue within the tumor and the strong induction of tumor immunity in that lymphoid tissue, suggesting that the underlying mechanism of this cytokine's anti-tumor activity may be effective. Therefore, LTα has long been considered to be a promising candidate for an anti-cancer agent. However, the clinical use of LTα has been limited because of the protein's *in vivo* instability and proinflammatory side effects.

One of the most common ways to improve the therapeutic effects of proteins is to conjugate them with polyethylene glycol (PEG) in a process called PEGylation, or to conjugate them with other water-soluble polymers [6]. Because of the steric hindrance caused by the PEG molecule, PEGylation can prolong the plasma half-life of molecules and alter the tissue distribution of the conjugates compared with those of the native form. PEGylation of proteins is mostly nonspecific because it targets all of the lysine residues in the protein, some of which may be in or near an active site. As a result, PEGylation significantly reduces the specific

Abbreviations: E. coli, Escherichia coli; ELISA, enzyme-linked immunosorbent assay; FADD, Fas-associated protein with death domain; FBS, fetal bovine serum; HVEM, herpes virus entry mediator; IFNγ, interferon γ; LTα, lymphotoxin-alpha; NFκB, nuclear factor-kappa B; PEG, polyethylene glycol; pI, isoelectric points; SDS–PAGE, sodium dodecyl sulfate–polyacrylamidegel electrophoresis; SPR, surface plasmon resonance; TNF, tumor necrosis factor; TNFR1, TNF receptor 1; TRADD, TNF receptor-associated death domain; TRAF, TNF receptor-associated factor; wtLTα, wild-type LTα.

* Corresponding authors. Addresses: Laboratory of Toxicology and Safety Science, Graduate School of Pharmaceutical Sciences, Osaka University, 1-6 Yamadaoka, Suita, Osaka 565-0871, Japan. Tel./fax: +81 6 6879 8233 (Y. Yoshioka), Laboratory of Biotechnology and Therapeutics, Graduate School of Pharmaceutical Sciences, Osaka University, 1-6 Yamadaoka, Suita, Osaka 565-0871, Japan. Tel.: +81 6 6879 8175; fax: +81 6 6879 8179 (S. Nakagawa).

E-mail addresses: yasuo@phs.osaka-u.ac.jp (Y. Yoshiokab), nakagawa@phs.osaka-u.ac.jp (S. Nakagawa).

[1] These authors contributed equally to the work.

1043-4666/$ - see front matter © 2012 Elsevier Ltd. All rights reserved.
http://dx.doi.org/10.1016/j.cyto.2012.11.005

activity of the proteins involved. Our group previously developed a novel strategy for site-specific mono-PEGylation of lysine-deficient mutants to overcome these limitations of PEGylation [7,8]. We demonstrated that site-specific PEGylation of a lysine-deficient mutant of LTα retained higher bioactivity compared with random PEGylation of wild-type LTα (wtLTα) [9]. This finding suggests that site-specific PEGylation of a lysine-deficient mutant of LTα might be a useful way to overcome the problems in the clinical use of LTα outlined above.

LTα binds to three receptor subtypes—TNF receptor 1 (TNFR1), TNFR2, and herpes virus entry mediator (HVEM)—to exert various biological functions. TNFR1 induces an anti-tumor effect and Peyer's patch development, whereas TNFR2 is essential for immune responses against bacteria and viruses [1]. Human LTα and TNF that bind to murine TNFR1, but not to murine TNFR2, are not lethal in healthy mice except at extremely high doses, suggesting that LTα and TNF α exhibit their lethal side effects *via* TNFR2 [10,11]. Therefore, LTα as a cancer immunotherapeutic agent, a LTα mutant with selectively increased TNFR1-mediated bioactivity is needed. Previously, we successfully created a TNFR1-selective LTα mutant whose bioactivity *via* TNFR1 was several times that of wtLTα, and whose bioactivity *via* TNFR2 was 2.5% that of wtLTα [12]. However, to enhance therapeutic efficacy and suppress the side effect of LTα, it is necessary to create a LTα mutant with greatly increased TNFR1-mediated bioactivity and TNFR1-selectivity.

In this study, we attempted to create LTα mutants with selectively increased TNFR1-mediated bioactivity by using a phage display technique. We succeeded in creating a LTα mutant that had a much higher bioactivity *via* TNFR1 and an augmented affinity to TNFR1 compared with that of wtLTα, and demonstrated that this was due to the slow dissociation rate of the LTα mutant-TNFR1 complex. In addition, we showed that the LTα mutant differed from wtLTα by its ability to strongly and rapidly activate caspases. In contrast, the LTα mutant and wtLTα were similar to each other in their degree of activation of nuclear factor-kappa B (NFκB). Our findings suggest that this LTα mutant would be a superior candidate for a cancer immunotherapeutic agent.

2. Materials and methods

2.1. Cells

HEp-2 cells, a human carcinoma cell line derived via HeLa contamination, were purchased from the American Type Culture Collection (Manassas, VA), and cultured in RPMI 1640 medium (Wako Pure Chemical Industries, Osaka, Japan) supplemented with 10% fetal bovine serum (FBS), 1 mM sodium pyruvate, 50 μM 2-mercaptoethanol, and antibiotics. HT29.14S cells, a TNF/LT-sensitive subclone of HT29 human colon adenocarcinoma, were kindly provided by Dr. Carl Ware (La Jolla Institute for Allergy and Immunology, CA) [13]. HT29.14S cells were cultured in Dulbecco's Modified Eagle's Medium (Wako Pure Chemical Industries) supplemented with 10% FBS, 10 mM HEPES, and antibiotics. hTNFR2/mFas-PA cells are preadipocytes derived from TNFR1$^{-/-}$ TNFR2$^{-/-}$ mice expressing a chimeric receptor composed of the extracellular and transmembrane domain of human TNFR2 and the intracellular domain of mouse Fas, which is a member of the TNF receptor superfamily [14]; these cells were cultured in RPMI 1640 medium supplemented with 10% FBS, 5 μg/mL Blasticidin S HCl (Invitrogen, Carlsbad, CA), and antibiotics. MCF-7 cells were provided from the Institute of Development, Aging and Cancer, Tohoku University, and were cultured in Eagle's Minimum Essential Medium (Wako Pure Chemical Industries) supplemented with 10% FBS, 0.01 mg/mL bovine insulin, and antibiotics.

2.2. Construction of a library of lysine-deficient mutants of LTα

The phagemid vector pY03′, which encodes human wtLTα with the C-terminus of wtLTα fused to the N-terminus of the M13 phage g3p, was used as a PCR template for constructing a DNA library of lysine-deficient mutants of LTα. We performed a two-step PCR amplification using oligonucleotides containing the sequence NNS (where N represents A, C, G, or T; and S represents C or G) at Lys19, Lys28, Lys39, Lys84, Lys89, and Lys119 of wtLTα; the sequence NNS encodes all 20 standard amino acids. The products from the second PCR were digested with *Nco*I and *Pst*I and then ligated into pY03′. The phagemid was electroporated into *Escherichia coli* (*E. coli*) TG1 cells (Stratagene, Cedar Creek, TX), yielding 2×10^6 independent clones. The phage library displaying lysine-deficient LTα molecules was prepared as described previously [12]. Briefly, pY03′-transformed TG1 cells were infected with M13KO7 helper phage (Invitrogen) and cultured for 6 h at 25 °C. The resultant phage particles were precipitated from the culture supernatant by using PEG (MP Biomedicals, Solon, OH) and suspended in NTE (100 mM NaCl, 10 mM Tris, 1 mM EDTA).

2.3. Selection of bioactive LTα mutants

Screening for bioactive LTα mutants was performed as described previously [12]. Briefly, an immunoplate was coated with soluble human TNFR1 (R&D Systems, Minneapolis, MN), and the prepared phage library was allowed to bind to the immobilized TNFR1. After a second round of panning, single colonies were picked and cultured. The resulting phage-containing culture supernatant was used for screening by enzyme-linked immunosorbent assay (ELISA) against human TNFR1.

2.4. Expression and purification of recombinant LTαs

pET15b plasmids (Novagen, Darmstadt, Germany) encoding LTαs were prepared and used to transform *E. coli* BL21(DE3) cells (Stratagene) for the expression of recombinant protein, as described previously [12]. Expression was induced by adding 1 mM isopropyl β-D-1-thiogalactopyranoside and incubating the cells at 37 °C for 6 h in Terrific Broth (Invitrogen Corporation, Carlsbad, CA) containing 0.4% glucose, 1.68 mM $MgSO_4$, and 100 μg/mL of ampicillin; all products were accumulated as inclusion bodies. The resultant inclusion bodies were washed, solubilized, reduced, and refolded by the methods previously described [12]. After dialysis against a buffer containing 20 mM Tris–HCl (pH 7.4) and 100 mM urea, active trimeric LTα proteins were purified by using a HiLoad Superdex 200PG column (GE Healthcare, UK) equilibrated with phosphate-buffered saline (pH 7.4) followed by ion-exchange chromatography (SP Sepharose Fast Flow for wtLTα; Q Sepharose Fast Flow for mutants of LTα); both columns were obtained from GE Healthcare. To create point mutants, we used pET15b-human wtLTα as a template with a KOD-plus mutagenesis kit (Toyobo, Osaka, Japan) according to the manufacturer's instructions. Recombinant point mutants were produced and purified as described earlier; SP Sepharose Fast Flow was used as the ion-exchange column. Protein concentration was measured by using Coomassie Protein Assay Reagent (Thermo Fisher Scientific, Rockford, IL). Sodium dodecyl sulfate–polyacrylamidegel electrophoresis (SDS–PAGE) analysis of LTαs was conducted under reducing conditions, and the proteins in the gels were stained with Coomassie brilliant blue. The electrostatic potential surface was generated by using GRASP software [15]. The electrostatic potential ranged from −7.5 kT to 7.5 kT. The relative accessible surface areas were calculated by using JOY software [16].

2.5. Cytotoxicity assays

HEp-2 cells were seeded at 4×10^4 cells per well in 96-well plates and incubated for 18 h with serially-diluted LTαs in the presence of 50 μg/mL cycloheximide. For the functional blocking assay, HEp-2 cells were treated with serially-diluted MAB225 (R&D Systems), an anti-TNFR1 antibody, for 30 min. The cells were then incubated with 100 ng/mL wtLTα and LTα mutants for 18 h in the presence of 50 μg/mL cycloheximide. For the caspase inhibition assay, HEp-2 cells were incubated with serially-diluted wtLTα or LTα mutants in the presence of 50 μg/mL cycloheximide and 50 mM zVAD-fmk (Calbiochem, Darmstadt, Germany) for 18 h. R2/Fas preadipocyte cells were seeded at 1.5×10^4 cells per well in 96-well plates and incubated for 48 h with serially-diluted LTαs in the presence of 50 μg/mL cycloheximide. The cytotoxicities of LTαs against HEp-2 cells and R2/Fas preadipocyte cells were assessed by using the standard methylene blue assay method as previously described [12]. HT29.14S and MCF-7 cells were seeded at 5×10^3 cells per well and incubated with LTαs in the presence of 80 U/mL human Interferon γ (IFNγ) (R&D Systems) for 72 h. After incubation, cell viability was measured by using a WST-8 assay kit (Nacalai Tesque, Kyoto, Japan) according to the manufacturer's instructions. The ratio of TNFR1-/TNFR2-mediated bioactivity was calculated as follows: activity of LTαs in HEp-2 cells/activity of LTαs in R2/Fas preadipocyte cells. The TNFR1/TNFR2 ratio for wtLTα was set equal to 1.

2.6. Analysis of binding kinetics by surface plasmon resonance

The binding kinetics of LTαs were analyzed and compared by using a surface plasmon resonance (SPR) method (BIAcore 2000, GE Healthcare, UK). Human TNFR1, TNFR2, or HVEM Fc chimera (R&D Systems, Inc.) was diluted to 50 μg/mL in 10 mM sodium acetate (pH 4.5) and immobilized onto a CM5 sensor chip by using an amine coupling kit (GE Healthcare, UK) as described previously [12]. During the association phase, wtLTα or LTα mutants diluted in HBS-EP running buffer (GE, Healthcare UK) to 37, 18.5, 9.3, 4.6, or 2.3 nM were passed over the immobilized TNFRs for 2 min at a flow rate 20 μL/min. During the dissociation phase, HBS-EP was run over the sensor chip for 1 min at a flow rate 20 μ L/min. Complexes were eluted by using 20 μL of 10 mM glycine–HCl (pH 2.0). Data were evaluated by using BIAevaluation 4.1 software (GE Healthcare UK) to apply a 1:1 Langmuir binding model. The obtained sensorgrams were fitted globally over the range of injected concentrations and simultaneously over the association and dissociation phases.

2.7. Evaluation of caspase-3/7 and -8 activities

HEp-2 cells were seeded at 4×10^4 cells per well in 96-well plates and then incubated for 6, 12, or 18 h with 10 ng/mL of the relevant LTα in the presence of 50 μg/mL cycloheximide. Activities of intracellular caspase-8 and caspase-3/7 were measured by using Caspase-Glo assays (Promega, Madison, WI) according to the manufacturer's instructions.

2.8. Evaluation of NFκB activities

HEp-2 cells were co-transfected with pGL4.32, a NFκB-responsive firefly luciferase expression vector, and pRL-TK, a thymidine kinase–regulated renilla luciferase expression vector (Promega) at a ratio of 90:1 for 18 h. The cells were then treated with 10 ng/mL of wtLTα or LTα mutants for 1, 2, 4, 6, 12, and 24 h. Expression levels of intracellular firefly luciferase and renilla luciferase were then measured by using the Dual-Luciferase Reporter Assay System (Promega). The expression level of firefly luciferase was normalized against that of renilla luciferase.

3. Results

3.1. Production of a highly bioactive LTα mutant

Our recent study showed that site-specific PEGylation of a lysine-deficient mutant of LTα might be useful for cancer therapy, because the mutant retained bioactivity after PEGylation [9]. Here, we attempted to create a lysine-deficient mutant of LTα with augmented bioactivity *via* TNFR1 and TNFR1-selective bioactivity that could be used for site-specific PEGylation in the future. A phage library displaying LTα mutants with randomized sequences in place of all lysine codons was prepared. For the construction of the phage library, two-step PCR was used to replace the lysine codons randomly with an NNS sequence. As a result, we successfully constructed a library with 2×10^6 independent clones, and performed two rounds of panning against immobilized human TNFR1; phage clones were screened for binding affinity to TNFR1 by conducting an ELISA (data not shown). We obtained three LTα mutants (mutLT1, mutLT2, and mutLT3), which were putative lysine-deficient mutants of LTα. DNA sequencing analysis of the LTα mutants confirmed that all 6 lysine residues present in wtLTα were mutated to other amino acids (Table 1). To investigate the properties of the LTα mutants in detail, we prepared recombinant LTα mutant proteins by using an *E. coli* expression system, as previously described [12]. LTα mutants and wtLTα were expressed in *E. coli* and obtained through refolding of inclusion bodies. Purified LTα mutants displayed a molecular mass of 18 kDa by SDS–PAGE analysis (Fig. 1A), and a molecular mass of approximately 60 kDa by size exclusion chromatography (Fig. 1B), indicating that LTα mutants form homotrimeric complexes, as does wtLTα. The isoelectric points (pI) of mutLT1, mutLT2, and mutLT3 were 6.16, 6.16, and 6.00, respectively whereas that of wtLTα was 8.94 (Table 1). We also visually assessed the changes in the surface electrostatic potential values by using GRASP software (Fig. 1C). Because of their lack of lysine residues, LTα mutants had more negative areas on their surface than did wtLTα.

3.2. Bioactivities of LTα mutants

To assess the TNFR1-mediated bioactivity of LTα mutants, cytotoxicity assays using HEp-2 cells were performed (Fig. 2A). wtLTα and LTα mutants showed dose-dependent cytotoxicity, and the bioactivity of each LTα mutant was higher than that of wtLTα in the HEp-2 cells (Fig. 2A). The bioactivity of mutLT1 was especially high (31.8 times that of wtLTα; Table 2). Furthermore, we confirmed that the LTα-induced cytotoxicity was blocked by the anti-TNFR1 antibody in all cases (Fig. 2B). These results indicate that the LTα mutants possess higher TNFR1-mediated bioactivity than that displayed by wtLTα. To confirm that the higher bioactivity of the LTα mutants was not specific to HEp-2 cells, we examined the bio-

Table 1
Amino acid sequences and the isoelectric points of LTα mutants. The pI values of LTαs were calculated by using a program in the Expert Protein Analysis System proteomics server of the Swiss Institute of Bioinformatics (Basel, Switzerland).

	Residue position						pI
	19	28	39	84	89	119	
wtLTα	Lys	Lys	Lys	Lys	Lys	Lys	8.94
mutLT1	Asn	Gln	Asn	Ser	Leu	Gly	6.16
mutLT2	Asn	Gln	Ser	Thr	Val	Val	6.16
mutLT3	Asp	Gln	Ala	Thr	Thr	Ala	6.00